Multiplexed Cell Analysis on CellCards™ for Drug Discovery

Ilya Ravkin*, Vladimir Temov, Aaron Nelson, Michael Zarowitz, Matthew Hoopes, Yuli Verhovsky, Gregory Ascue, Simon Goldbard, Oren Beske, Bhagyashree Bhagwat, Holly Marciniak
Vitra Bioscience, 2450 Bayshore Parkway, Mountain View, California, 94043

ABSTRACT

The desire to obtain more biologically relevant data is expanding the use of cell-based assays in drug discovery. These assays are performed and analyzed in ever more sophisticated ways (e.g. high content screening) that allow the collection of multiparametric information about cells affected by the screened compounds. The driver for these developments is the desire to increase data quality and density and reduce the use of valuable reagents and time.

Here we describe an approach that adds a new dimension to the data quality/quantity mix by simultaneously analyzing several cell types in the same microplate well. The system is based on the use of encoded carriers (CellCards®) that permit the reading and analysis of cellular responses, and at the same time allow decoding and the attribution of these responses to the appropriate cell line. CellCards are rectangular particles with an expandable color barcode and a transparent section upon which cells can be grown and imaged for cellular readout. Before performing the assay, each cell line is grown on a different class of CellCards. CellCards, with attached cells, are mixed and dispensed into a microtiter plate where the assay is performed. Next the plates are imaged, decoded and the cells associated with each CellCard class are analyzed.

Multiplexing cell lines allows assay controls and data normalization within each well, reducing well-to-well variability. It also allows the simultaneous interrogation of multiple targets and thus concurrent potency and selectivity screening. This may significantly reduce the time required to take a compound from primary screening into the clinic.

Keywords: multiplexed cell analysis, encoded carriers, selectivity screening

1. INTRODUCTION

Many new technologies seek to increase both the density and quality of the data, gathered from experiments. Microarray technologies, both positional and non-positional[1,2,4,5], have provided an efficient way to achieve this. Multiplexing experiments within a single well increases information density by simultaneously obtaining data on multiple analytes within a single well[3,5]. The increase in data quality and robustness is derived from the ability to include internal controls and to correlate data obtained from identical reaction conditions[5]. The non-positional array technology presented here provides, for the first time, a platform that enables this type of analysis to be done with a diverse set of cellular assays.

A common approach to miniaturizing cell-based assays in the drug discovery industry is to reduce the reaction volume in which the assays are performed. This not only decreases the volume and cost of the reagents used, but also increases the throughput of the operation. However, this approach requires expensive liquid handling equipment and a significant amount of time to re-optimize the assay to the new conditions. The CellCard technology effectively miniaturizes assays without the need for low-volume liquid handling and reformatting of the assay. That is, if we assay ten cell lines in the same reaction volume that is typically used for a single cell line, that volume becomes ten times more efficient. We have proven repeatedly that cell lines multiplexed on CellCards and grown independently in plates behave indistinguishably, provided they are at the same level of confluency[6].

* iravkin@vitrabio.com

The CellCard platform is compatible with a diverse set of cellular assays. These assays range from biochemical in nature, i.e. cytokine capture, to live cell assays requiring extended incubation with compound. By enabling the performance and analysis of such diverse assays, the use of this technology may provide a unique insight into the profiling of compounds for potency, selectivity, and mechanistic activities.

2. ENCODED CARRIERS

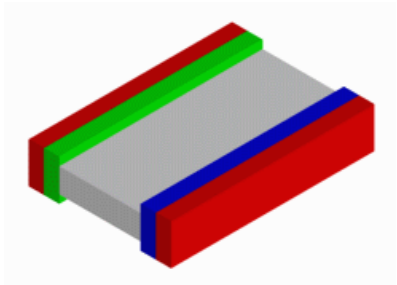

Fig. 1. CellCard with two coding bands on each side and a recessed clear cell readout area in the middle.

Encoded cell carriers, CellCards, are the basis of the cellular multiplexing platform presented here. These particles have embedded in them a positional code that is optically readable. In addition, they can support the growth of cells and are usable for optical imaging of cells. The configuration of CellCards depends on the desired number of classes (codes), on the preferred manufacturing methods, on the detection modalities of both the code and the cells, and on the format of the system (e.g., slides, microtiter plates of given density, etc.).

The current design separates the area of the particle that is used for encoding from that used for biological readout. The latter is the useful area and the former is the overhead of encoding. Since the code within each particle is positional, it can use as few as two distinguishable states (e.g., colors). The number of coding positions (e.g., bands) is then chosen to encode the required number of classes.

Fig.1 shows a CellCard in conceptual form. The particles have an aspect ratio that causes them naturally to lie flat. Since in practice a CellCard may lie either side up, the number of distinguishable codes is given by the following formula:

$N_D = (N_T - N_S)/2 + N_S$, Where N_D is the number of distinguishable codes, N_T is the total number of codes, N_S is the number of symmetrical codes. For more reliable recognition we impose an additional restriction that adjacent bands can not be of the same color. With this: $N_T = (M(M-1))^2$, $N_S = M(M-1)$, where M is the number of colors. Thus, if three colors are used for the coding bands, $N_D = 21$. This number of distinguishable classes is sufficient for cellular multiplexing in 96-well microtiter plates.

The carriers have overall dimensions of L=500µm, W=350µm, H=100µm. The recess of the middle area provides better cell retention during dispensing and diffusion of reagents during the assay phase. The carriers are made of biocompatible materials and demonstrate no cellular toxicity.

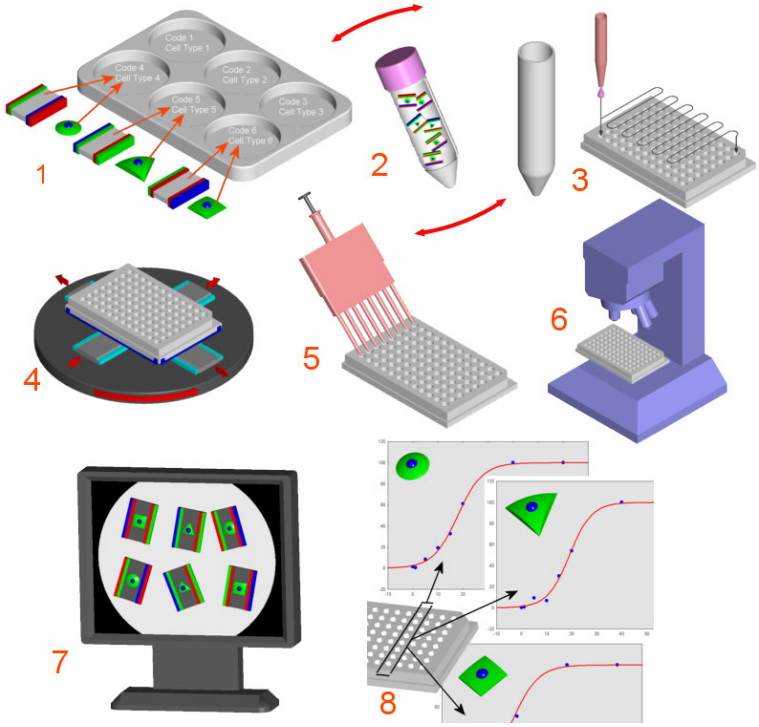

Fig. 2. Procedure for performing assays on CellCard carriers: 1-plating cells on carriers, 2-mixing, 3-dispensing, 4-dispersing, 5-performing the assay, 6-image acquisition, 7-image analysis for decoding and cell measurements, 8-data analysis.

3. PROCEDURE FOR PERFORMING ASSAYS ON CELLCARDS IN MICROPLATES

3.1. Overview

The diagram in Fig. 2 illustrates the steps of performing an assay on CellCard carriers. 1) The carriers are dispersed in 6-well plates, the cells are plated onto of the carriers and incubated overnight to allow cells to attach and spread; 2) the carriers with attached cells are combined and mixed; 3) approximately 100 carriers are dispensed from the mixing tube into each well of a microtiter plate; 4) the carriers are dispersed to minimize overlaps; 5) the assay is performed as usual; 6 - images of each well are acquired in both brightfield and fluorescence mode; 7) images are analyzed to decode the carriers and make assay-specific measurements; 8) numerical well-level data is analyzed and plotted.

3.2. Dispensing

The transfer of a homogeneous mixture of CellCard particles carrying multiple cell lines to an assay plate is an essential step in the screening process using the CellCard system. It requires minimizing shear forces that might detach cells while maintaining the hydrodynamic and surface tension forces that are used to transfer the CellCards from the dispensing container to the microtiter wells. The CellCard dispenser (Vitra Bioscience, Mountain View, CA) is based on a syringe-driven liquid handling system. Custom tips and accurate liquid control ensure proper transfer of the particles. The CellCard dispenser is optimized to enable recognition by the software of the largest number of carriers. Too many carriers would cause overlaps and reduce recognition. The maximal number of recognized CellCards in a 7-mm well is around 100 and it can be achieved with around 110 dispensed CellCards (the counts were produced after dispersing, see below).

3.3. Dispersing

The goal of dispersing is to provide a single layer of CellCards in order to minimize overlap, and thereby maximize the number that can be recognized by the software. Although the particles are small, their density is more than twice that of the solution in which they are dispensed, so they sink rapidly to the bottom. Once in the wells, the particles rest in a random clustering as seen in Fig. 3 (left). The CellCard disperser uses two orthogonal bearings mounted to an orbital shaker to convert the orbital motion of the shaker to the linear motion required for dispersion. Speed, distance of travel, and the amount of liquid in the well have been optimized for best dispersion. An example of CellCards before and after dispersion is shown in Fig. 3.

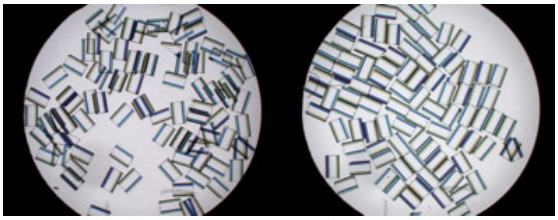

Fig. 3. Left - Carriers in a well before dispersing, Right - same well after dispersing

4. IMAGING OF CELLCARDS

Imaging of CellCard carriers poses some specific challenges caused by the thickness of the particles and by the need to image the whole well. To this end, we have developed the CellCard Analyzer (Vitra Bioscience, Mountain View, CA), to enable brightfield illumination (for decoding), focusing, and fluorescence imaging of whole wells with CellCards that have cells both “face up” and “face down”.

4.1. Brightfield imaging

Shadow-free illumination of carriers in the whole well is created in the system by a custom integrating sphere with 24 color LEDs. This configuration provides sufficient light intensity to achieve integration times from 1 to 3ms. Switching time is < 1ms. The light from the LEDs is reflected from the diffuse white interior of the integrating sphere, thus illuminating the top of the sphere uniformly. This area of the sphere provides illumination to the well that is uniform

from all angles, as well as uniform throughout the field of view. This is the ideal illumination condition for brightfield microscopy, and is optimal for reading the code bands.

4.2. Fluorescence imaging of cells on CellCards

When cells are initially grown on CellCards (before dispensing them in the 96 well plate) they are all on the top surface of the particles. However, after mixing and dispensing the carriers can land with the cells in either orientation: up or down. This has implications for the staining and subsequent imaging of the cells. The current design of the carriers (Fig. 1) has a recessed area to achieve good diffusion of reagents under the carrier to the cells on its bottom surface. The carriers are made of a material that does not introduce optical distortions; the middle section is clear with parallel surfaces and the thickness of 30-50µm, which is 3-5 times thinner than a coverslip. Compared with the thickness of the bottom of a microtiter plate (0.7 mm for the 96-well Viewplate, Packard Biosciences; Boston, MA, used here) the added thickness is not significant. However, the particles add two more interface surfaces. Fig. 4 shows two carriers in the same well imaged at top and bottom surfaces. Our experience shows that there is no image degradation when imaging through the carrier at objective magnifications from 2X to 20X. We also did not observe any consistent or significant difference in the intensities of images from the top and bottom surfaces of the carriers.

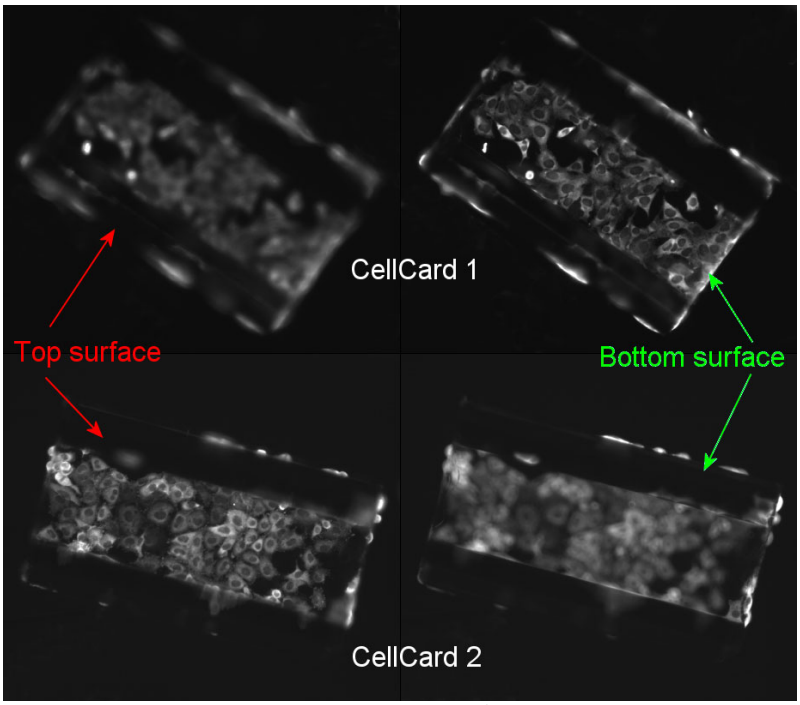

Fig. 4. Two carriers imaged at top and bottom surfaces with a Nikon Plan Fluor 10X 0.3NA objective.

5. RECOGNITION AND DECODING OF CELLCARDS

The ability to recognize and decode CellCards is at the core of this platform. The RGB image, after its background has

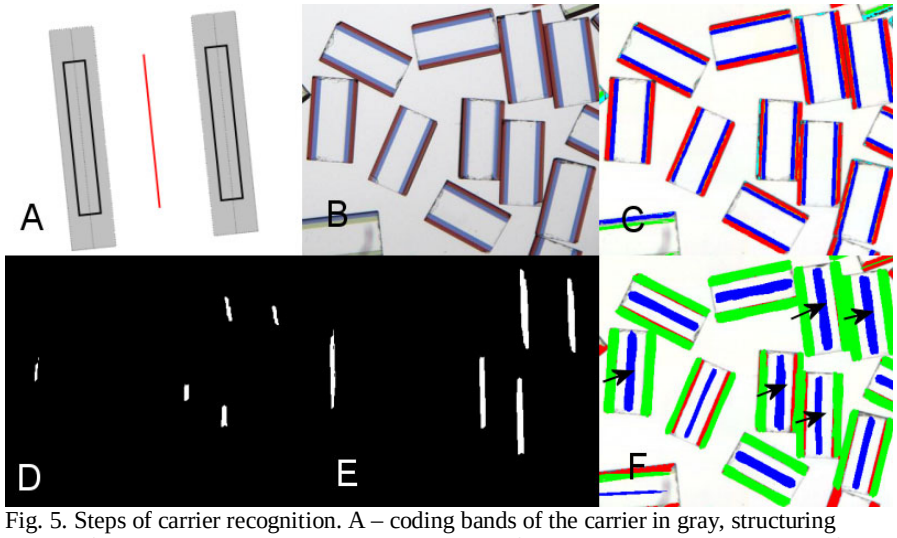

Fig. 5. Steps of carrier recognition. A – coding bands of the carrier in gray, structuring element for erosion in black and structuring element for dilation in red shown at one of the orientations, B – fragment of a well image before background equalization, C – color masks, D – erosion of band mask by structuring element of A produces carrier markers, E – dilation of carrier markers of D by structuring element of A produces medial lines of carriers, F – carriers with coding bands and medial lines produced after pattern matching at all orientations where carriers of orientation shown in A, D and E are indicated by arrows.

been equalized, is converted to hue, saturation, value (HSV) color space. A color mask is produced for each of the colors used in the coding bands of the carriers. Color masks are joined into the band mask, which is used for detection of carriers.

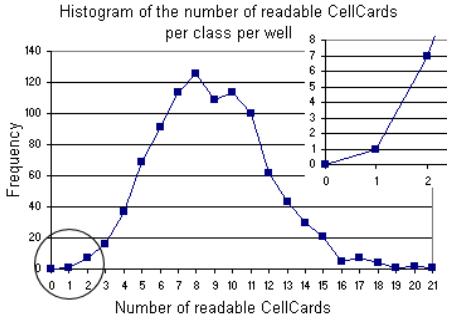

Fig. 7 A typical histogram of the number of readable CellCards per cell type per well (for 10 classes in each well). The inset shows in larger scale that there are no wells with 0 carriers and one well with 1 carrier per cell type. This data point may be removed as unreliable.

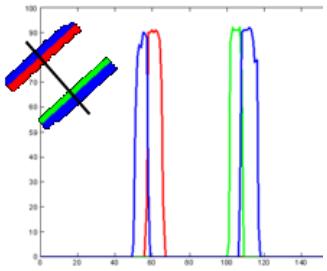

Fig. 6. Color bands and their projections. Code BR-GB

CellCards appear in the image as a disjoint pair of double color bands at random orientations. The model of a carrier image is shown in gray in Fig 10 A. The detection of carriers is based on erosion of the band image by the structuring element shown in black in Fig 10 A. This structuring element is a pair of rectangles of a length that is smaller than the shortest CellCard and a width that is about half the width of the coding band. The result of such erosion – carrier markers - is shown in Fig. 5 D. The marker image is dilated by the structuring element shown in Fig. 5 A in red giving medial lines of carriers (Fig 5 E). This process is repeated for the orientations of the structuring element from 0° to 180° with 4° step. The medial lines from all orientations are accumulated and shown together with band masks in Fig. 5 F.

After all CellCards are detected, those that are too short, broken or are overlapping other CellCards are rejected. The algorithm has the option of retaining the non-overlapping portions of overlapping CellCards, which is useful for some assays. Since the CellCard image is at this stage a disjoint set of two coding bands there is a chance that a space between two CellCards may be misidentified as a CellCard. To prevent this, a check is performed to ensure that each coding band belongs to only one CellCard.

When the location and orientation of each CellCard is known, the algorithm calculates the projection (number of pixels) of each of the color masks on the direction perpendicular to the medial axis of a CellCard. These projections are shown in Fig.6. The sequence of color peaks in the plot gives the code. In addition, the measurement mask is produced for each

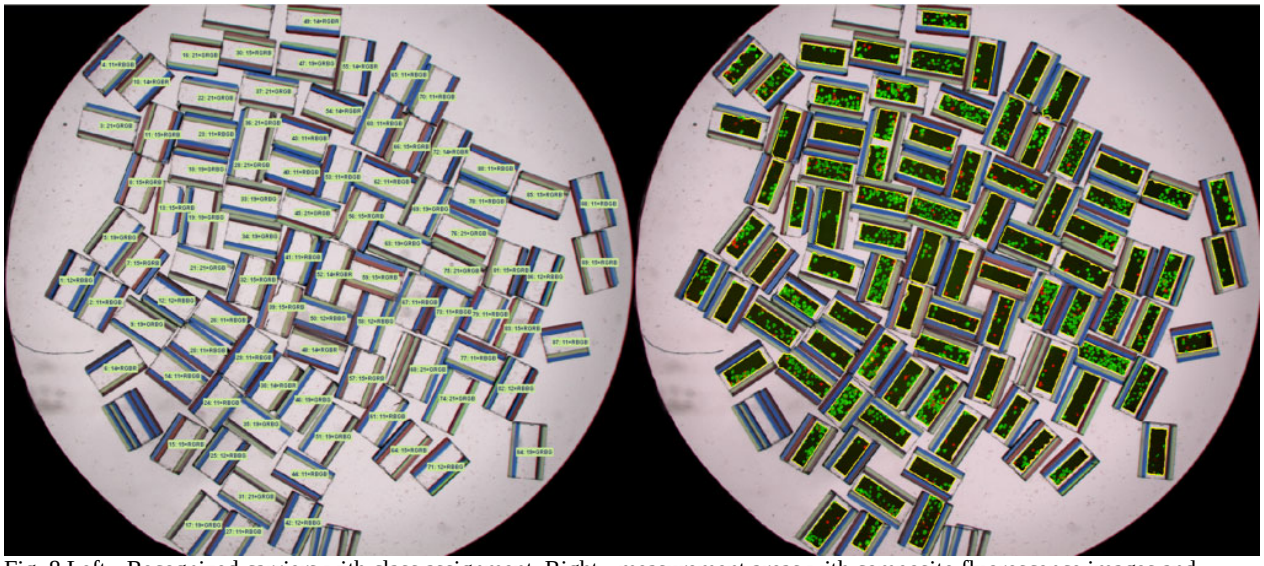

Fig. 8 Left - Recognized carriers with class assignment, Right - measurement areas with composite fluorescence images and overlaid contours inscribed into each carrier. Note that overlapping carriers and those partially in the image are neither recognized nor used for cell measurements.

CellCard. Results are represented visually to the user in the format shown in Fig. 8. A representative distribution of the numbers of CellCards in a well for each of the 10 classes is shown in Fig. 7. The CellCard recognition software as well as cell analysis software described below is implemented using Matlab (MathWorks, Natick, MA) and its Image Processing Toolbox.

6. ANALYSIS OF CELL IMAGES ON CELLCARDS

In the CellCard platform, the means to deconvolve the mixture of cell types residing on different CellCard classes is the decoding of the carriers through the analysis of their brightfield images. The cellular measures, however, are derived from images of cells, which are typically fluorescent. We have imaged cells on CellCards with intrinsic fluorescence (e.g., GFP), cells stained with fluorescence-conjugated antibodies, cells stained with colorimetric dyes, and even unstained cells. Here we will concentrate on the analysis of fluorescent cell images. As described above, the CellCard platform is based on utilizing and analyzing all available well area. Thus, the desire is to work at the lowest possible magnification in order to attain the greatest throughput. The lowest possible magnification is determined by the demands of cell image analysis and depends on the assay. In this paper we give examples of two assays, Mitotic Index and S-phase Index, and determine their image resolution requirements.

In cellular imaging assays, the measure (or measures) used to characterize the assay is far removed from the signal registered by the camera. Different algorithms will produce different assay measures on the same image. This is especially acute for redistribution assays (e.g., nuclear translocation) where the total intensity may not change and the assay result may depend more on the algorithm than on the raw image. In order to decide which resolution is minimally acceptable for a given assay and algorithm we analyze the same well area at different optical magnifications or/and the same set of images at different interpolated magnifications. In a similar manner, the effect of the cell number is analyzed by comparing measures from images of different size. To compare results we use quality functions discussed in the next paragraph.

6.1 Assay and algorithm quality measures for cell-imaging assays

In high throughput drug screening it is common to evaluate the quality of assays by a statistical parameter that depends on the dynamic range and variability of the assay. Several such parameters have been introduced with z-value[7] being the most popular. Z-value is given by the following formula:

$Z = 1 - 3(\frac{SD_{pos} + SD_{neg}}{|M_{pos} - M_{neg}|})$, where SD is standard deviation, M is mean, *pos* and *neg* are the two extreme states of the assay, which define its dynamic range. Z value ranges from $-\infty$ to 1. For cell-based assays, z-values above 0.5 are considered good. Other common parameters are also based on the means and standard deviations of the positive and negative states of the assay. These measures proved to be very useful to capture and compare variability caused by assay biology and by instrumentation (e.g., pipetting). Cell assays based on imaging introduce several new variables: imaging resolution, size of the imaged area and the data extraction algorithm. Imaging resolution in a camera-based system practically means optical magnification. Size of the imaged area is a variable because usually less than the whole well is imaged and analyzed. Having a quality measure, like the z-value, allows us to optimize variables that are under our control, e.g., find the best data extraction algorithm.

In addition to introducing new variables, cellular imaging assays may lead us to reconsider the quality measure itself. An assay measure derived from an image may be computationally very complex. It may contain operations that have the effect of saturating the values from the positive and negative states of the assay, thus artificially reducing variability. This may happen unintentionally and even without being realized. Moreover, if the values of the assay for its positive and negative states do not overlap (and if they do it may not be a very useful assay), the z-value can be manipulated intentionally, by applying a mathematical transformation that maps all positive values into a single value and all negative values into another single value, which would result in z-value of 1. One way of dealing with this is the use in the quality measure of a dose-dependent sequence of assay states (dose-curve) with doses being close enough to each other, so that artificial manipulation would be impossible. This leads to the following measure, which we refer to as the "v-value":

$V = 1 - 6(\frac{SD_{of\_fit}}{|M_{pos} - M_{neg}|})$, where $SD_{of\_fit} = \sqrt{\sum_{1}^{n} \frac{(f_{exp} - f_{mod})^2}{n}}$, f_{exp} and f_{mod} are experimental and model values of the assay measure at a given concentration, n is the number of experimental points in the dose curve.
The v-value reverts to z-value if there are only two dose points. The model may be chosen depending on the nature of response, with logistic curves often being the natural choice. Alternatively, as is the case with the examples given below, no specific model is used and the average of several replicas is used as f_{mod} in the above equation.

The v-value is less susceptible to saturation artifacts caused by computation than z-value. There is also another subtle difference. Standard deviation in the middle of the dose-response curve is often larger than the standard deviation at the extremes. This is because the maximal point on the curve is often determined at saturating concentration, and so any dispensing error has little effect on the response; the minimal point is usually zero concentration and it also avoids dispensing errors. In contrast, the effect of volume errors has its maximal effect in the middle of the dose-response curve. Taking the whole curve into account gives a more realistic measure of the assay data quality.

6.2 Measures of cell proliferation

We will study here several image-derived measures that can be used to characterize cell proliferation. The Mitotic Index assay, which is commonly used in anti-cancer drug discovery, is used as an example. This assay uses two fluorescent stains. One stain labels the nuclei of every cell. This stain is used as a counter stain and represents a measure of all cells present. The second stain is a fluorescent antibody that labels only those cells in the mitotic phase of the cell cycle. Cell proliferation is assessed here by two types of measures: 1) estimate of the cell number, and 2) estimate of the percent of cells in mitosis (mitotic index). Each of these types of measures can be numerically expressed by different algorithms. We will consider two algorithms for each type of measure and study their behavior as a function of magnification and image size (number of cells).

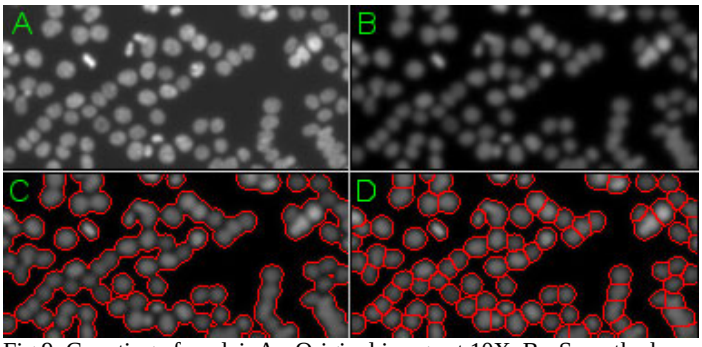

Fig 9. Counting of nuclei: A - Original image at 10X, B - Smoothed image, C - Smoothed image with adaptive threshold contours, D – Same contours with watershed separation lines inside.

The most direct estimate of the cell number is achieved by counting of nuclei on the counter stain image. This is done by the following algorithm: 1) Background removal based on morphological opening[8]. 2) Magnification-dependent smoothing by a combination of morphological openings/closings and convolution with a smoothing kernel. The amount of smoothing is empirically chosen as a tradeoff between oversegmentation and undersegmentation by watershed. 3) Adaptive threshold by Otsu's method[11], which chooses the threshold to minimize the intraclass variance of the black and white pixels. 4) Watershed[9,10] of the inverted smoothed image to separate touching nuclei. An example of an image processed by this algorithm is shown in Fig. 9. Other measures of the cell number can be obtained by measuring areas or intensities of nuclei in the counter stain image. These measures may be produced by an algorithm similar to the one, described above, except that the step of separating of the touching nuclei is not necessary and the measures are taken on original and not on

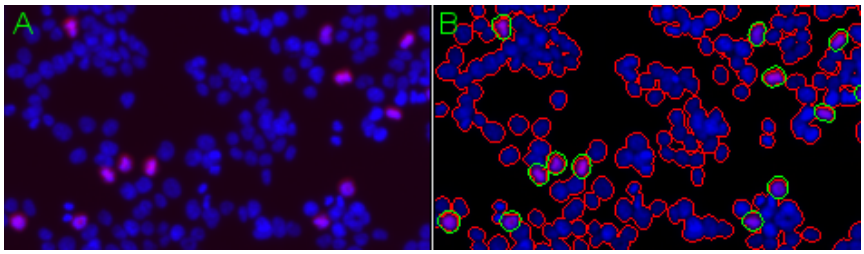

Fig. 10. Image of Mitotic Index assay. Counter stain is rendered in blue and signal stain is rendered in red. Adaptive threshold contours for the counter stain are in red and for the signal stain are in green. A – original image, B – same image with contours.

smoothed images.

Estimates of the mitotic index may be based on the measures described above, with the index being the ratio of the measures from the signal stain and from the counter stain. Fig. 10 shows an image of Mitotic Index assay with contours representing counter stain areas and signal stain areas used to calculate these measures. The following measures were studied: A) Nuclear count per mm^2, B) Percent of area occupied by nuclei, C) Ratio of signal stain area to counter stain area, D) Ratio of signal stain intensity to counter stain intensity. The data for this study was a set of eight wells in a microtiter plate corresponding to different doses of the drug Paclitaxel affecting HCT116 cell line. Two sets of images were acquired from the eight wells. One set was acquired at objective magnification of 10X, another at objective magnification of 2X. The dose curves for these measures are shown in Fig. 11.

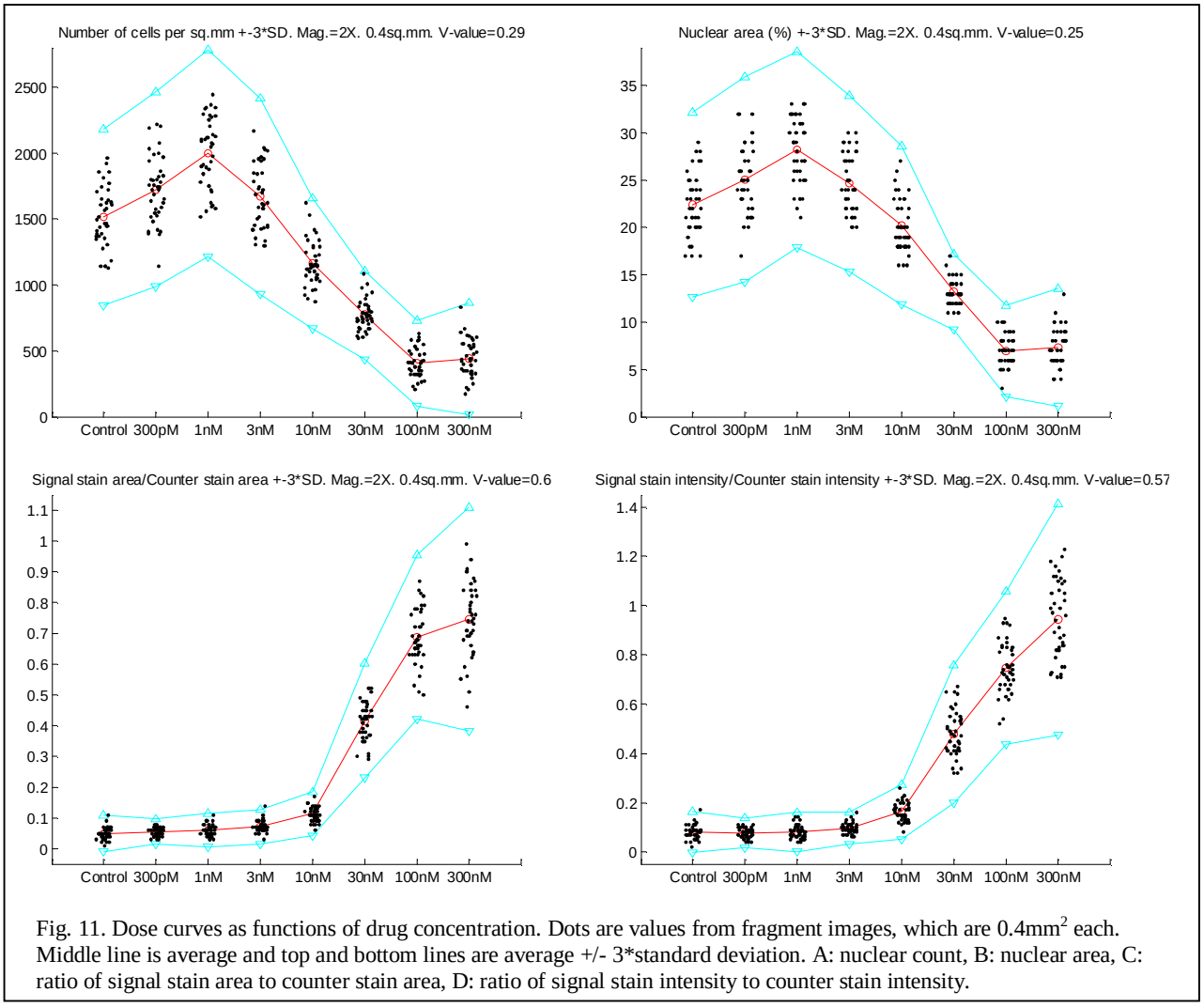

Fig. 11. Dose curves as functions of drug concentration. Dots are values from fragment images, which are 0.4mm^2 each. Middle line is average and top and bottom lines are average +/- 3*standard deviation. A: nuclear count, B: nuclear area, C: ratio of signal stain area to counter stain area, D: ratio of signal stain intensity to counter stain intensity.

In the first part of the study we used the 10X images; the variables were interpolated image magnification (from 10X down to 1X), and image size. The v-value concept introduced above was used as a measure of quality. In the v-value formula we used average standard deviation around the mean at each drug concentration. Image interpolation was done by the bilinear method. To study image-size dependency, the original image at each dose was divided into fragment images of smaller sizes. Each of the smaller images was used to produce the four measures, which in turn were used in the formula for v-values.

The dependency of v-value on image size and magnification is shown in Fig. 12. It is quite clear from the plots that magnification between 10X and 2X has little effect on the quality of all four measures. At the same time, there is a very strong dependency of the quality on the image size. Relative measures (C,D) are far less dependent on image size than absolute measures (A,B).

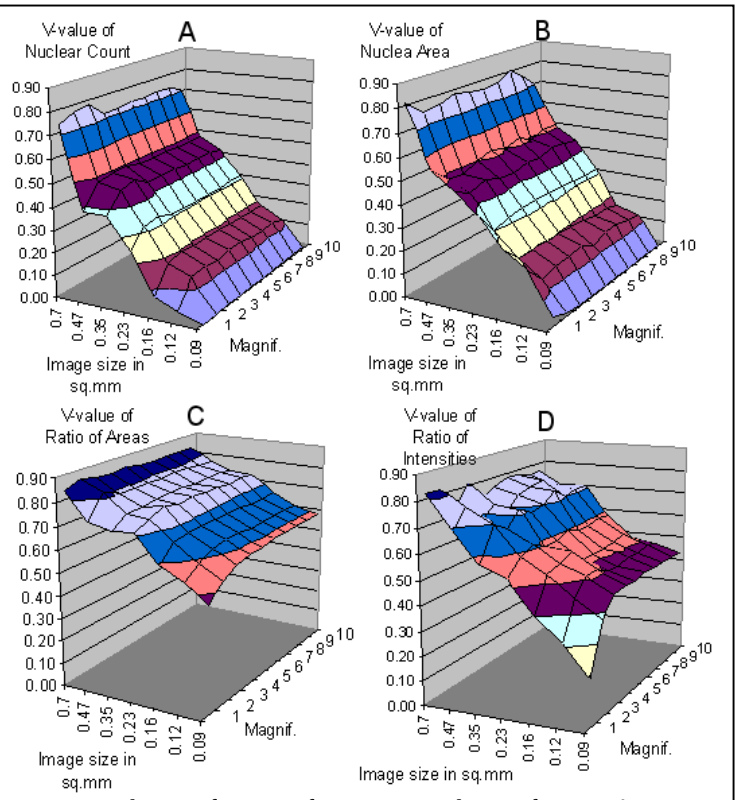

Fig. 12. V-value as a function of image size and magnification: A: nuclear count, B: nuclear area, C: ratio of signal stain area to counter stain area, D: ratio of signal stain intensity to counter satin intensity.

In the second part of the study we fixed magnification at 2X and analyzed the dependency of v-values on the image size alone using images covering much larger area in the well – 16mm^2 instead of 1.4mm^2. The result is shown in Fig. 13. The ratio of areas is the measure used in the Mitotic Index example below.

Most of the assays that we perform on the CellCard platform use at least two stains. One of the stains is typically a counter stain; it labels the nucleus or plasma membrane. The other stain or stains label the "signal". They are typically localized within the compartment, which is labeled by the counter stain. The use of two stains makes it possible to calculate derivative measures. These measures can be quite complex, as in nuclear translocation assay[12], or they can be simple ratios of the measures for each of the stains as described above. The advantage of using relative measures is not only that they have a clear biological meaning, but also that they are more stable. The image size at which v-values reach acceptable range for the relative measures may be an order of magnitude smaller, than for the raw measures, such as cell count (Fig. 13 shows that v-value of 0.6 is reached at image size of 0.4mm^2 for relative measures and only at image size of 4mm^2 for raw measures). Therefore, the relative measures are more appropriate in the miniaturized environment.

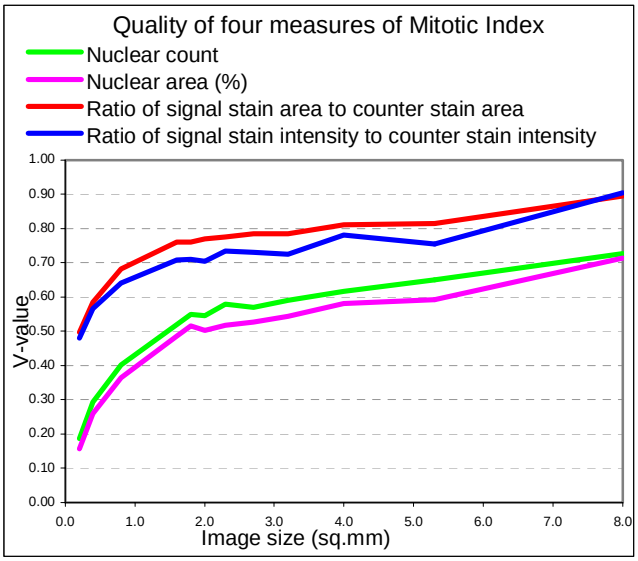

Fig. 13. V-values of four measures of cell proliferation at magnification 2X as a function of image size.

We have developed a general methodology to determine bounds within which cellular imaging assays have acceptable behavior. Here we have applied this methodology to determine image resolution and image size requirements for several measures of cell proliferation and to choose the best measures.

Several other sources of variability can be easily identified, such as variation in staining, in camera acquisition parameters, in the light source, in the user-settable parameters of the data extraction algorithm. These factors may change from well to well, from plate to plate, from day to day, or from

operator to operator. The study of these factors was outside the scope of this article. It is important to note, thought, that we use only data extraction algorithms that do not depend on proper parameter setting by the user. Even without conducting a study it is clear that measures (even relative measures) based on intensity values are more susceptible to staining, camera and light source variation than measures based on areas determined by adaptive thresholds. Most importantly, successful analysis of these dependencies rests on a good measure of quality. We believe that the v-value introduced above, combined with a proper dose-response model provides such a measure.

7. MULTIPLEXING CELL-BASED ASSAYS USING CELLCARDS

The graph shown in Fig. 14 demonstrates one type of multiplexed data that may be generated using the CellCard system. Ten cell lines from different tissues were assayed in each microtiter well using the Mitotic Index assay as described above. The Mitotic Index represents the portion of the cellular population that was in the mitotic phase of the cell cycle when the cells were stained. Since each cell type has a unique steady state Mitotic Index, the data is normalized to a negative control. That is, we divide the experimental value by the negative control value. Therefore, experimental treatments that have no effect result in a Mitotic Index of one, while treatments that increase the proportion of cells in mitosis have a measure greater than one and those that decrease the proportion of cell in mitosis have a value of less than one.

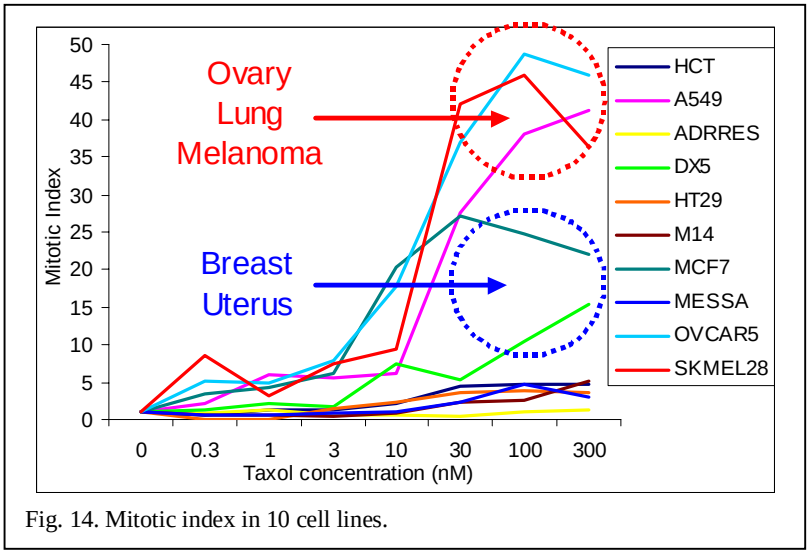

Fig. 14. Mitotic index in 10 cell lines.

The experiment was designed to profile both the activity and selectivity of Taxol, a commonly used anti-tumor drug, with respect to tissue of origin. Taxol is an agent that is known to increase the proportion of cells in mitosis. Therefore, it is expected that the Mitotic Index would rise as a function of Taxol concentration. The cell lines at the bottom of the plot show little or no response to this agent. Conversely, the outlined cell lines demonstrate varying levels of response. The responses of these cells range from relatively sensitive to the compound (Ovary, Lung, Melanoma - in the top circle) to intermediate (Breast, Uterus - in the bottom circle). Since the cell lines were multiplexed on carriers, at each dose, each cell line experienced identical assay conditions. Taken together, these data show how differential cellular responses (selectivity) to a potential therapeutic agent can be profiled with a high degree of assurance that these differences are not due to assay errors.

Next, we applied this technology to another cell-based assay relevant for anti-cancer drug discovery, a brominated-deoxy-uracil (BrdU) incorporation assay. This assay is designed to measures the cellular event of DNA synthesis, associated with the synthesis phase (S-Phase) of the cell cycle, as a measure of proliferation. The quantification of this assay is very similar to that described above for the Mitotic Index assay. Briefly, there are nuclear and BrdU incorporation specific stains. The ratio of the BrdU stain to the nuclear stain results in a measure of the S-Phase Index of the cellular population. This measure has also been normalized in the same way as the Mitotic Index assay but is expressed as a percentage of the negative control. Experimental treatments resulting in no effect on the S-Phase Index result in a value of one hundred percent whereas treatments that stimulate cellular proliferation increase the S-Phase Index to a value of greater than one hundred and treatments that inhibit cellular proliferation result in values of less than one hundred. This assay is designed to measure cellular health and proliferative capabilities. Another approach is simply the counting of the number of cells as described above. Therefore, we have also chosen to use a quantification of the nuclear stain alone as an assay measure. In this case the data is normalized differently. A separate set of three wells is fixed and stained prior to incubation with test compounds. This serves as a time zero control and represents the number of cells present at the beginning of the incubation. We divide our experimental values by this value to obtain

the Relative Growth measure. In doing such, treatments that result in no net growth, a cytostatic situation, show a Relative Growth value of one. Treatments that allow a net growth in the cellular population return values of greater than one, while those that induce cell loss result in values less than one. The result is an assay that returns two cellular parameters for each cell type in the well from the same set of images. In other words, this assay results in twenty data points being simultaneously generated from each individual microtiter well when multiplexed by ten cell lines.

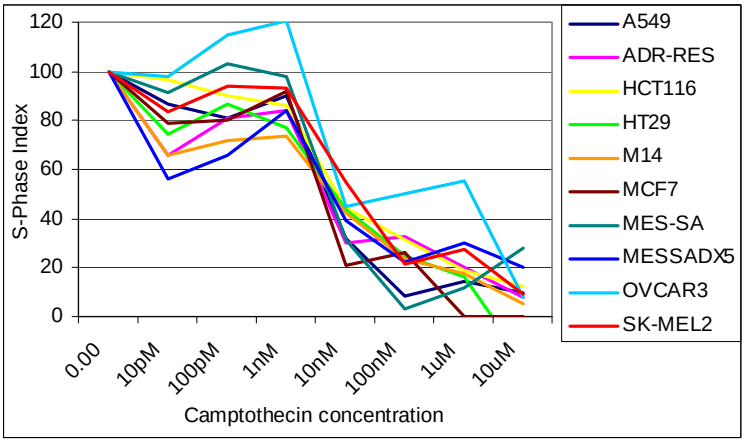

Fig. 15. S-Phase Index from BrdU-incorporation assay in 10 cell lines (in %).

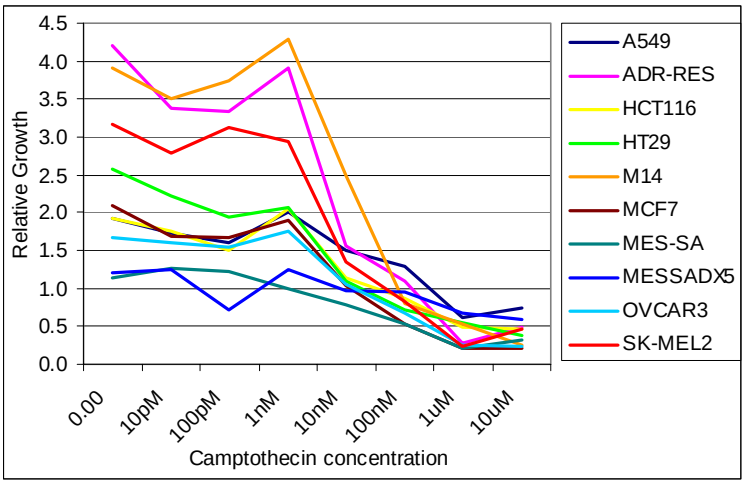

Fig. 16. Relative Growth from BrdU-incorporation assay in 10 cell lines.

In this experiment ten cell lines, again representing different tissues of origin, were treated with increasing doses of the anti-prolierative drug Camptothecin. As expected, there is a dose-dependent decrease in the S-phase Index (Fig. 15) and in the Relative Growth (Fig. 16). The effects of this drug on the S-Phase Index and on the Relative Growth are similar. Specifically, the drug doesn't seem to have any effect on the cellular population at doses of less than 1nM. As the drug concentration increases above 1nM there is a dramatic reduction in both parameters. A closer look at the data reveals some subtle biological nuances. For example, the S-Phase Index graph shows that for some cell types there is a plateau at concentrations greater than 100nM while for other cell types the Index continues to decrease. There are similar differences in the Relative Growth response. Of note is the fact that the concentration required to induce a cytostatic environment (Relative Growth equal to 1) varies by greater than 100 fold between the cell types. These subtle cell-type specific differences, which we term selectivity, are important criteria used to asses potential therapeutics. By implementing the CellCard technology to gather this information, these differences can be identified in a more robust manner, and much earlier in the drug development process. As previously described, since the data for each cell type was generated simultaneously from a single well, there is no possibility that these cell-type specific differences were due to other factors, such as well-to-well variability introduced by pipetting errors.

8. CONCLUSION

We have developed the CellCard System as a means of miniaturizing cell-based assays in the drug discovery industry. This technology enables multiple cell lines to be assayed in a single well in 96-well microtiter format. This results in scalable savings in assay reagents with the number of cell lines multiplexed. If ten cell lines are assayed, the reagent savings is ten-fold. In addition, any variability introduced by pipetting or other sources, is greatly reduced. Since all of the cell lines in a given well have experienced identical conditions there can be no day-to-day, plate-to-plate, or well-to-well variation. This ensures that each data point can be unequivocally compared to each other from the same well. Internal well controls may also be employed. That is, CellCards may be used to read-out assay specific steps such that any errors in the assay could be identified and flagged. This technology enables drug discovery laboratories to profile

compounds for their activity and selectivity simultaneously. Miniaturization through the use of CellCards not only gives quantitative benefits of lower cost and higher throughput; it may enable experiments that could not otherwise be contemplated. As an example, when the cells to be screened are limiting, as is often the case with primary cells, use of the CellCard system reduces cell consumption by up to two orders of magnitude and makes possible screens of high predictive value.

REFERENCES

1. Nolan, J.P. & Mandy, F.F. “Suspension array technology: new tools for gene and protein analysis”, *Cell Mol Biol* **47**, 1241-1256, 2001.
2. Zhou, H., Roy, S., Schulman, H. & Natan, M.J. “Solution and chip arrays in protein profiling”, *Trends Biotechnol* **19**, S34-39, 2001.
3. Iannone, M.A. et al. “Multiplexed molecular interactions of nuclear receptors using fluorescent microspheres”, *Cytometry* **44**, 326-337, 2001.
4. Armstrong, B., Stewart, M. & Mazumder, A. “Suspension arrays for high throughput, multiplexed single nucleotide polymorphism genotyping” *Cytometry* **40**, 102-108, 2000.
5. Martins, T.B. “Development of internal controls for the Luminex instrument as part of a multiplex seven-analyte viral respiratory antibody profile”, *Clin Diagn Lab Immunol* **9**, 41-45, 2002.
6. O. Beske, J. Guo, J. Li, D. Bassoni, K. Bland, H. Marciniak, M. Zarowitz, V. Temov, I. Ravkin, S. Goldbard "A novel encoded particle technology that enables simultaneous interrogation of multiple cell types", *J. Biomol. Screening*, 2004 (in press).
7. J.-H. Zhang, T.D.Y. Chung, K.R. Oldenburg “A simple statistical parameter for use in evaluation and validation of high throughput screening assays”, *J. Biomol. Screening* ***4***: pp. 67-73, 1999
8. J. Serra, *Image Analysis and Mathematical Morphology*, Vol. 1. Academic Press, London, 1989
9. S. Beucher and F. Meyer, “The Morphological Approach to Segmentation: The Watershed Transformation” in: *Mathematical Morphology in Image Processing*, E.R. Dougherty – Ed., pp. 433 – 481, Marcel Dekker, New York, 1993
10. L. Vincent, P. Soille, "Watersheds in Digital Spaces: An Efficient Algorithm Based on Immersion Simulations", *IEEE Transactions of Pattern Analysis and Machine Intelligence*, **13**, No. 6, pp. 583-598, 1991
11. N. Otsu "A Threshold Selection Method from Gray-Level Histograms," *IEEE Transactions on Systems, Man, and Cybernetics*, ***9***, No. 1, pp. 62-66, 1979
12. I. Ravkin, et al. "Multiplexed high-throughput image cytometry using encoded carriers", *Proceedings of SPIE* (Manipulation and Analysis of Biomolecules, Cells, and Tissues) Vol. 5322, 2004 (in press)